Naval Research Laboratory
Washington, DC 20375-5320

NRL/6390/MR—2021/5

Nanotopographical Influence on Cell Behavior

MICHAEL C. ROBITAILLE

Center for Materials Physics and Technology
Materials Science and Technology Division

May 25, 2021

REPORT DOCUMENTATION PAGE

Form Approved
OMB No. 0704-0188

1. REPORT DATE *(DD-MM-YYYY)*	**2. REPORT TYPE**	**3. DATES COVERED** *(From - To)*
25-05-2021	NRL Memorandum Report	01/10/2019 – 30/09/2020

4. TITLE AND SUBTITLE

Nanotopographical Influence on Cell Behavior

5a. CONTRACT NUMBER

5b. GRANT NUMBER

5c. PROGRAM ELEMENT NUMBER
NISE

6. AUTHOR(S)

Michael C. Robitaille

5d. PROJECT NUMBER

5e. TASK NUMBER

5f. WORK UNIT NUMBER
N2V2

7. PERFORMING ORGANIZATION NAME(S) AND ADDRESS(ES)

Naval Research Laboratory
4555 Overlook Avenue, SW
Washington, DC 20375-5320

8. PERFORMING ORGANIZATION REPORT NUMBER

NRL/6390/MR--2021/5

9. SPONSORING / MONITORING AGENCY NAME(S) AND ADDRESS(ES)

Naval Research Laboratory
4555 Overlook Avenue, SW
Washington, DC 20375-5320

10. SPONSOR / MONITOR'S ACRONYM(S)

NRL-NISE

11. SPONSOR / MONITOR'S REPORT NUMBER(S)

12. DISTRIBUTION / AVAILABILITY STATEMENT

DISTRIBUTION STATEMENT A: Approved for public release; distribution is unlimited.

13. SUPPLEMENTARY NOTES

Karle Fellowship

14. ABSTRACT

The wound healing process is a complex cascade of events, recruiting different cell types that receive precise instructions through a variety of physical cues. One such cue involves cellular response to the underlying substrate topography, ranging from the nano- to microscale. However, the fundamental mechanisms throughout this process are still poorly understood, largely due to the fact that cellular response in-vitro is extremely context dependent. Additionally, heterogeneity amongst experimental platforms further confounds results between research groups. Here, we outline a novel fabrication method to impart highly reproducible nanotopographical cues in SiO2 coverslips that are readily integrated with all forms of live-cell microscopy, can easily scale up for manufacturing, and are well characterized in terms of surface roughness and protein adsorption. The SiO2 topography chips are validated on fibroblasts, a crucial cell type in the wound healing process, and fibroblast adhesion and migration in response to topographical cues is investigated.

15. SUBJECT TERMS

16. SECURITY CLASSIFICATION OF:			**17. LIMITATION OF ABSTRACT**	**18. NUMBER OF PAGES**	**19a. NAME OF RESPONSIBLE PERSON**
					Michael C. Robitaille
a. REPORT	**b. ABSTRACT**	**c. THIS PAGE**	SAR	16	**19b. TELEPHONE NUMBER** *(include area code)*
U	U	U			(202) 767-5654

This page intentionally left blank.

CONTENTS

This page intentionally left blank.

NANOTOPOGRAPHICAL INFLUENCE ON CELL BEHAVIOR

INTRODUCTION

Wound Healing and Topography

The cells that comprise our tissues and organs are responsible for the development, maintenance, remodeling and repair of that tissue. They are able to do this in part by measuring and responding to the physical properties of their local environment, the *extra cellular matrix* (ECM, i.e. tissue), in a highly efficient and organized manner. When a wound occurs and disrupts the natural architecture of the ECM, it also alters its physical properties. The ensuing process to heal the wound is a complex cascade of events in which different cell types are recruited and receive precise instructions through a variety of physical and chemical cues from their local environment. One such cue involves cellular response to the underlying substrate topography, known as contact guidance. Contact guidance has been shown to play crucial roles in wound healing[1], as well as other biological processes such as development[2] and cancer metastasis[3]. For instance, early in the wound healing process fibrin clots provide contact guidance cues for fibroblast migration, proliferation and secretion of new matrix during Fibroplasia[1]. Through sensing the topography of their underlying environment, cells respond by altering their morphology, adhesion, migration and ultimately function. However, the fundamental mechanisms throughout this process are still poorly understood.

The Naval Research Laboratory (NRL) conducted this research to elucidate underlying mechanisms of cellular response to topographical cues to help guide the design of next generation wound healing materials. Learning from fundamental biological processes offers an appealing avenue for material design of enhanced wound healing technologies that could improve recovery and functionality to accelerate the Reintegration of the Wounded Warrior – a top priority of the Navy and the DoD in general. By understanding how cells respond to topographical cues in a reproducible manner, it is possible to optimize wound healing material properties to utilize these cues to encourage the desired cellular response at various stages in the wound healing process (i.e. enhanced migration into the wound bed).

A New Topographical Platform

Various research groups have investigated cellular response to topographical properties over the years by taking advantage of advances in micro/nano-fabrication techniques to construct in vitro platforms. Substrates are fabricated with a range of topographical feature sizes and geometries, and are subsequently coated with ECM proteins or peptides to promote cell adhesion, mimicking in vivo environments and tissues. Despite large research efforts spanning years to examine cellular response to topographical cues, it remains difficult to see general trends in the literature. This is largely due to the fact that cellular response to environmental cues is heterogeneous in nature, and further more often depends upon the context in which the cues are presented to the cells. In terms of topography, the resulting cell behavior varies dependent upon the cell type[4], and even within a given cell type the in vitro conditions can directly alter the cellular response. For instance, Teixeira *et al.* have shown that simply using different culture media can drastically change cellular orientation to identical topographical cues[5], highlighting a crucial aspect of topographical platforms often overlooked – the material surface interface. Indeed, the importance of the surface interface of in vitro platforms is well appreciated in the field of cell biology, and two key aspects that are known to influence cell behavior are protein adsorption and surface roughness[6, 7]. However, out of the dozens of topographical studies reviewed in[8, 9], only five studies characterized surface roughness[10-13] and two studies characterized protein adsorption[14, 15]. In addition to a typical lack of surface characterization amongst topography platforms, the sheer diversity in materials and

Manuscript approved May 3, 2021.

methods used for platform fabrication further confounds comparisons amongst different studies, making general trends slow to apprehend.

This program aims to establish a standard in vitro platform and to characterize cellular responses to topographical cues. The NRL is uniquely capable of helping establish such a research platform by virtue of its multidisciplinary scientific scope and state-of-the-art nanofabrication facilities at the Nanoscience Institute. By leveraging such nanolithographic resources, we outline a novel fabrication protocol that offers an in vitro platform with tight control in terms of topographical features, surface roughness and characterized protein adsorption on commercially available SiO_2 substrates. The platform has a multiplexed format and can readily integrate with live-cell microscopes across different magnifications and modalities, making it ideal as a standard experimental set up to address heterogeneity of topographical platforms within the research community. A series of chips were fabricated with range of topographical parameters, and validated by characterizing the morphological and migrational response of Hs27 fibroblast cells across a range of optical modalities.

APPROACH

A Multiplexed Nanotopography Chip

Here, we introduce a monolithic SiO_2 nanotopography chip to help address the heterogeneity amongst platforms, as well as their environmental and surface ambiguity in vitro. The benefits of utilizing commercially available SiO_2 coverslips as a substrate offers many advantages. First, the nanotopography chip is able to integrate with a fluidic-environmental chamber and various live-cell microscopy modalities. Second, SiO_2 surfaces allow for biofunctionalization via standard silane chemistry approaches as well as protein adsorption characterization via Quartz Crystal Microbalance with Dissipation (QCM-D), offering a window into the surface conditions that contribute to the environmental context of any in vitro assay. Third, the SiO_2 surface is able to be regenerated via application of standard enzymatic reagents and surfactants as well as plasma-ashing, allowing a single chip to be re-used indefinitely. To our knowledge, there is no proposed "standard" platform to characterize how a cell type responds to topographical cues – somewhat surprising given the 1) known physiological importance of topographical cues, 2) the attention in-vitro topographical platforms have garnered over the years, and 3) the general concern of a lack of reproducibility in biological research.

Fluidic Environmental Platform

The key design criteria for a fluidic environmental platform are ease of integration with nanotopography chips and conventional in vitro experimental setups while maintaining consistent in vitro conditions including temperature, CO_2 level, and concentration of cell media. Any changes in the in vitro conditions during the experiments could alter cell response. In order to achieve the goals, we developed the fluidic environmental platform shown in Figure 1. A custom fluidics assembly was designed for adequate heat transfer, high-magnification microscope compatibility, and is interchangeable for various multiplexed SiO_2 nanotopography chips, shown in Figure 1A-B. The assembly has three main components: An aluminum base for adequate heat transfer at 37°C in environmental chambers/stages atop microscopes, a 25 mm diameter silicon backing ring to add structural support to the 1 inch diameter patterned coverslip substrate, a #1.5 (170 μm) fused silica coverslip (SPI Supplies, GE124) that serves as the substrate for the chip topographies, a 250 μm thick silicone gasket and a biocompatible polycarbonate reservoir (Makrolon) with fluidic input and output channels for controlled fluid/reagent swaps that are designed to eliminate bubble formation. The entire platform can be sterilized via ethanol baths and assembled aseptically in a biosafety hood, and support high-magnification (100x) live-cell microscopy for over 72 hrs.

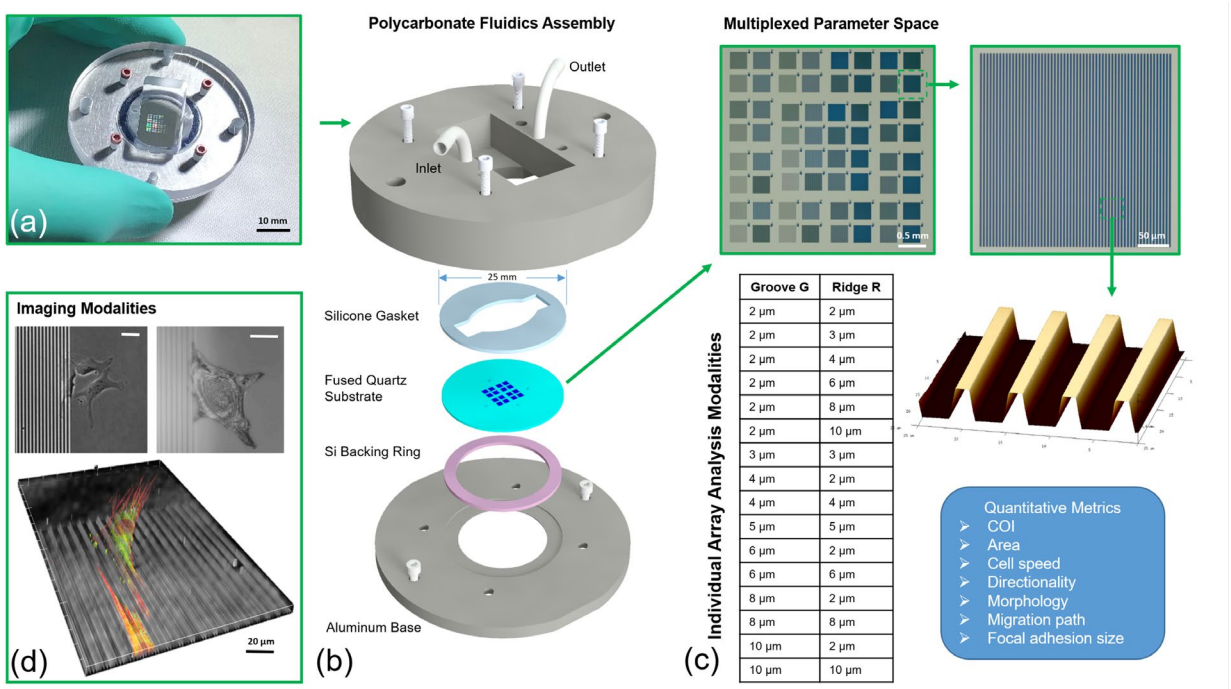

Fig. 1 — SiO_2 Nanotopography Platform. A) Entire assembled platform. B) Exploded view of polycarbonate fluidics assembly highlighting components geared towards tight environmental control for extended life-cell microscopy. C) Overview of multiplexed topographical layout highlighting 64 field of views (FOV) covering 16 different topographies (top left) and a single FOV covering a single topography (top right). Table summarizing groove (G) and ridge (R) dimensions covered on the nanotopography chip with a single etch depth d =725nm (middle). Box highlighting quantitative metrics to characterize cellular response (bottom). D) The platform is compatible with a wide range of optical modalities – common phase contrast (top left), IRM (top right), and confocal microscopy (bottom).

Chip Fabrication

The fabrication of the nanotopography chip was optimized to create multiplexed chips with a smooth (i.e. low roughness) and uniform surface, as variations in local roughness could alter cellular response and surface functionalization. A 20 nm Cr thin film was e-beam evaporated onto 25 mm diameter fused silica coverslips and subsequently coated with AZ1518 photoresist (Microchemicals GmbH) and baked on a vacuum hot plate at 100°C for 90 seconds. The photoresist was patterned in a Heidelberg VPG200++ laser pattern generator at a dose of 60 µC/cm^2. The samples were developed using AZ developer (Microchemicals GmbH) and rinsed in deionized (DI) water. The resist pattern was transferred into the underlying Cr film by chrome wet etch using CR-7 (KMG Electronic Chemicals, Inc.) for 15 seconds and rinsed in DI water. The patterned Cr film acted as hard mask, allowing only the exposed fused silica area to be etched (Oxford PlasmaLab 100 ICP380 system) by CHF_3 and Ar, with flow rates of 10 and 15 sccm, respectively, at 3 mTorr and 20°C. Each patterned 25 mm fused silica sample was placed onto the center of a four-inch Si carrier wafer with a 5 µl drop of fomblin oil sandwiched in between to assist with heat dissipation. The RIE RF power applied was 20 W (at 13.56 MHz) and the ICP power was set to 600 W (at 2 MHz) to achieve an etched depth of d = 725 nm. The remaining resist was removed using a Plasma Preen O_2 system, and residual Cr was removed via CR-7 for 5 minutes followed by copious DI water rinse. The silicon backing ring and the silicone gasket (Figure 1B) were shaped from a 550 µm thick Si wafer and a 250 µm thick silicone sheet respectively, using an E-355 Oxford Laser micromachining system. The patterned fused silica coverslip offers a relatively large area suitable for nanotopography fabrication (7×7 mm^2), allowing for a wide range of topographical conditions to be implemented in a single chip, summarized in Figure 1C.

Chip Characterization

Atomic Force Microscopy (AFM) was used to characterized surface topography and roughness across the chips. All AFM imaging was conducted on a Dimension FastScan (Bruker) in either Peak-force tapping mode with ScanAsyst Air probes or tapping mode with FastScan-A probes (Bruker). Topographical scans were collected at 512x512 resolution for smaller scans to measure surface roughness, while larger survey scans for height, width and pitch measurements were collected at 1024x1024 resolution. All scans were done in ambient conditions. For a given chip, a fresh probe was used to measure RMS roughness at four locations across the chip. Both the etched SiO2 (bottom grooves, G) and virgin SiO2 (top ridges, R) were measured at each location. For Fibronectin (FN) adsorption characterization, Human plasma FN (Gibco, Prod # 33016105) was diluted down to a concentration of 25µg/mL in 10mM PBS. To reduce large globular aggregates that could potentially interfere with the topography, the FN was spun down at 6,000 rpm/1600 g for 5 min, and carefully aspirated to avoid larger particulates at the bottom of the centrifuge tube. The FN was drop coated directly onto chips and allowed to adsorb for 1 hr at room temperature, followed by 3 rinses with double deionized water (DDW) and dried under gentle N2 stream and subsequently imaged.

All protein adsorption measurements were conducted on a Qsense Analyzer (Biolin Scientific) on Qsensor QSX 303 SiO_2 sensors (Biolin Scientific). Prior to each test, the SiO_2 sensors were cleaned by hydrogen plasma ashing via Technics RIE (40 W, 300mTorr, 45 seconds). The sensors were immediately inserted into each flow cell and allowed to equilibrate under running 10mM PBS buffer, waiting for each sensor to have less than 1 Hz drift/hour. Once each sensor was equilibrated under running buffer, 25 µg/mL of FN was introduced for 1 hour at a flow rate of 100µL/min, and subsequently rinsed afterward with buffer to remove any lightly bound FN from the adsorbed layer. The subsequent frequency and dissipation shifts were fit using a Voight viscoelastic model [16] to estimate the amount of adsorbed material on the SiO_2 surface and resulting film thickness in the QTools software (Biolin Scientific). Experiments were conducted in triplicate.

In vitro Experiments

For validation of the integrated, multiplexed chips, we performed a series of in vitro experiments using fibroblast cells as a model. For cell culture, Hs27 cells (ATCC, CRL-1634, Lot #7006836) were cultured in DMEM (ATCC, 30-2002) with 10% FBS (ATCC, 30-2020, Lot #802500) at 37°C and 5% CO2 as per manufacturer instructions, without antibiotics. The cells were monitored in real-time via Incucyte (Essen Biosciences) to calculate confluence and growth curves as a function of passage. A noticeable shift in growth curves was observed at passage 9, an indicator of senescence, and thus only passages 4-8 were used for experiments.

For live cell experiments, the topography chips and surrounding chambers were assembled under aseptic conditions. Ethanol was introduced to the chambers for 5 min and then N2 dried for additional sterilization of the chips. FN at 25µg/mL in 10mM PBS was drop coated directly onto the chips and allowed to adsorb for 1 hr at room temperature, and subsequently rinsed 5x with DMEM to remove any excess FN. The set up were then allowed to equilibrate on Zeiss microscopes featuring environmental chambers at 37°C, 5% CO2 and 95% humidity for at least 30 min before the introduction of cells. Hs27 cells were harvested for experiments between 30-60% confluence, in their logarithmic growth phase. Complete media was aspirated and replaced with 0.25% Trypsin-EDTA (Gibco, #25200-056) for 5 min at 37°C, after which serum free media was introduced. Cell viability (>90%) and density were then measured via Trypan Blue stain, and approximately 5,000-10,000 cells were drop coated directly onto each chip. Each set up was then sealed with sterile CO2 permeable films (4titude, #4ti-0518/ST) that prevent evaporation of media from the chamber during experiments. Migration studies were conducted under 10x phase microscopy, and for high-resolution 40x IRM was used.

Regions of interest (ROI) were selected across each chip for areas containing cells, and images were taken every 10 min. Cell migration was tracked via ManualTracking ImageJ plugin by tracking the cell nucleus between time-frames. Only cells that exhibited a migration track longer than 6 hours were considered for analysis, and a cell track ended when the nucleus was no longer on the topographical structures. Cells that underwent mitosis were not analyzed. The total distance of a single cell track was calculated based off of the individual (x, y) coordinates of the cell nucleus over all time steps of that track. The cell velocity was calculated as the total distance traveled of a track divided by the total time of that track. The cell directionality was calculated as the distance of the final (x, y) coordinates of a track divided by the total distance traveled by that track. Cell morphology was extracted manually in ImageJ from phase contrast imagery to obtain cell area, which was then fit to an ellipse from which the aspect ratio and orientation angle were calculated. All topographies were oriented at 90°. To characterize orientation, the Cell Orientation Index was defined as:

$$\mathrm{COI} = 2\left[\sin\varphi - {}^{1}/_{2}\right];\ 0° \le \varphi < 180°$$

such that the average COI of ellipses oriented parallel to the topographies equals 1. A Mann-Whitney test was used to test for statistical significance (* $p < 0.05$, ** $p < 0.005$), and all boxes in plots represent the 1st to 3rd quartile with a whisker length of 1.5 the inter-quartile range.

Immunostaining, when combined with fluorescence microscopy, is a powerful tool to visualize specific biological molecules associated with certain cellular functions. Because focal adhesions and stress fibers are relevant to cellular mechanisms that mediate cell migrations, we demonstrated that immunostaining techniques can be directly utilized with our chips. At the end of an experiment (~18 hrs), the cells were fixed for immunostaining. The chip was carefully washed three times with PBS, and then incubated with 4% paraformaldehyde (Electron Microscopy Science) in PBS for 10 min, followed by three more PBS washes. The cell membranes were then treated with 0.1% Triton X-100 in PBS for 10 min before incubating with blocking buffer (3% BSA (ThermoFisher Scientific, 37525) + 10% normal goat serum (NGS, ThermoFisher Scientific, #31873) + 0.1% Tween 20 in PBS) at room temperature for 1 hr. Subsequently, cells were incubated with diluted mouse monoclonal anti-vinculin (1 to 500 dilution) (Sigma-Aldrich, #V9131) in 3% BSA + 10% NGS in PBST at room temperature for 1 hr. After washing the cells with PBST six times and then PBS three times, cells were then incubated with anti-mouse IgG conjugated with DyLight488 (Jackson ImmunoResearch Laboratory Inc, #715486151) at room temperature for 1 hr before washing with PBST and PBS. To stain nuclei, cells were then incubated with 5 µg/mL of DAPI (Sigma-Aldrich, #D9542) at room temperature for 15 min. To stain actin, cells were treated with fluorescent dye rhodamine phalloidin (ThermoFisher Scientific, #R415) for 30 minutes according to the manufacturer's protocol. Immunostained images were analyzed via CellProfiler [17] to extract morphological parameters of focal adhesions in an automated fashion between different experimental conditions

The cells, their secreted proteins, and adsorbed proteins were cleaned off the quartz surface after a live-cell experiment by two methods. For experiments that did not involve fixation with paraformaldehyde for immunostaining, chips were rinsed with copious amounts of 1% Enzol detergent (Johnson & Johnson) followed by PBS + 0.5% Tween20 (T20). Afterwards, the chips were incubated with a mixture of 0.25% trypsin-EDTA with 0.5% Triton X-100 (Sigma, #T8787) for 1 hr at 37°C. Chips were then further rinsed with 1% Enzol, PBS + 0.5% T20, and then DDW before being dried under gentle N2 streams. Chips were monitored under dark field microscopy to assess for any contaminants or residues left over. For experiments that did involve fixation for immunostaining, chips underwent the same regeneration protocol listed above, but received an additional O2 plasma clean via Technics RIE (100 W, 300mTorr, 120 seconds).

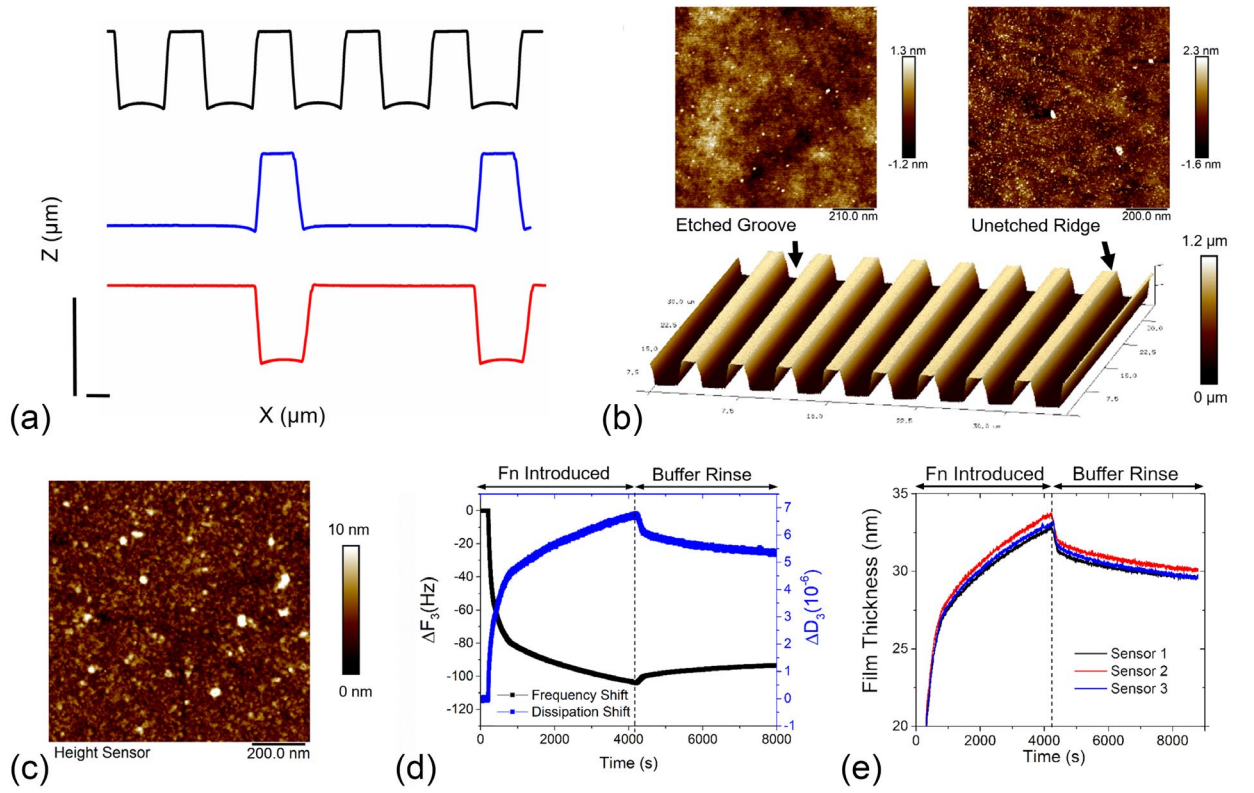

Fig. 2 — SiO_2 Nanotopography Chip Characterization. A) AFM cross-sections of the three topographical conditions (scale bars = 1 µm). B) Roughness measurements of the etched grooves and unetched ridges. C) AFM characterization of adsorbed fibronectin (FN) on flat SiO_2 portions of the nanotopography chip. D) QCM-D measurements highlighting the 3rd harmonic shift in frequency and dissipation for 25 µg/mL FN on bare SiO_2. E) Corresponding adsorbed FN film thickness estimates.

EXPERIMENTS

SiO_2 Nanotopography Characterization

Here we characterized the surface roughness and protein adsorption of the SiO_2 topography chip using AFM and QCM-D techniques, respectively. Figure 2 shows the characterization of the chip topography and SiO_2 surfaces. Roughness was taken across the chip on both the unetched top ridges and etched bottom grooves to ensure there were no significant differences between the two surfaces that could affect protein adsorption. Top ridges had Ra = 0.51 ± 0.25 nm and bottom grooves had Ra = 0.53 ± 0.12 nm, shown in Figure 2B. Given the size of FN, a 220kDa globular protein approximately 6 nm by 60 nm before considering aggregates [18], differences in roughness values would likely have to be well over a nanometer to have a significant effect on adsorption to the SiO_2 surface. FN adsorption onto the SiO_2 surfaces at a concentration of 25 µg/mL was characterized by AFM, shown in Figure 2C. At this concentration, FN densely aggregated on the surface, exhibiting spherical-like domains ranging from ~20-50nm in diameter, increasing the surface roughness to Ra = 0.74nm. No isolated domains or aggregates were observed, indicating that the FN established complete surface coverage.

The combined shifts in the frequency and dissipation were used to evaluate the amount of FN adsorbed to the SiO_2 surfaces via QCM-D, with a representative Δf_3 and ΔD_3 vs. time response shown in Figure 2D. 25 µg/mL of FN was allowed 1 hr to adsorb onto the surface, during which the 3rd harmonic

frequency shifted by ~ -100Hz. A buffer rinse was applied to remove loosely bound FN and mimic the in-vitro functionalization protocol, stabilizing the frequency shifts at ~ -90Hz. To estimate the thickness of the adsorbed FN film, the 3rd-11th harmonic of both frequency and dissipation shifts were fitted to a Voight model assuming a uniformly thick, homogeneous FN layer in the QTools software [16]. After rinsing with buffer, the remaining FN film adsorbed to the SiO_2 surface was estimated to be 29.8 ± 0.3 nm thick.

We next demonstrate how this multiplexed chip and assembly design enables high data throughput while remaining compatible with commonly used microscopy modes for both live and fixed cell imaging. Due to the sheer size and complexity of data generated from a single multiplexed chip experiment (64 individual experiments yielding 18 hours of diverse time-lapse imagery, Figure 1C-D), four conditions are initially analyzed to screen for influences of topography on Hs27 fibroblast behavior. As validation of this platform, the following topographies were analyzed for fibroblast morphology, migration, and focal adhesion characterization: G = 2 μm/R= 2 μm (G=2 R=2), G = 2 μm/R= 8 μm (G=2 R=8), and G = 8 μm/R= 2 μm (G=8 R=2), shown in Figure 2A. Flat surfaces in between etched topographies served as on-chip controls.

Cellular Response to Nanotopography

Cell Morphology

Fibroblasts were observed to respond quickly to all SiO_2 topographies, with initial alignment to etched grooves occurring in as little as 10 minutes within initial attachment to the surface. Cell morphology was measured approximately 6 hours after initial plating to characterize fibroblast response to the SiO_2 topography. All topographies resulted in high degrees of cellular alignment, with the Cellular Orientation Index (COI) for each topographical condition showing a tight distribution around an average value of approximately 1, indicating high degrees of alignment when compared to flat SiO_2 controls (Figure 3A). The fibroblasts on each topography were categorized by their number of lamellipodia; two for an elongated cell morphology, three for a triangular-like morphology, and four or more for cells with a more complex, spread out morphology (Figure 3D). Fibroblasts on the smaller topographical features (G=2 R=2) almost exclusively exhibited a two-lamellipodia elongated morphology compared to the more spread out flat SiO_2 controls (85% versus 16%, respectively, Figure 2D). Topographies with wider grooves or ridges (G=2 R=8 and G=8 R=2) exhibited an increase in fibroblasts with three and four or more lamellipodia, indicating that topographical constraints confine lamellipodia formation at this depth. Fibroblasts on flat SiO_2 controls had a significantly larger area compared to all groove/width topographies studied (Figure 3B). Cells on topographies with a ridge width of R = 2μm exhibited an aspect ratio of about twice as much cells on flat SiO_2 controls or topographies with wider ridges (R = 8μm, Figure 3C, Figure 5A-F).

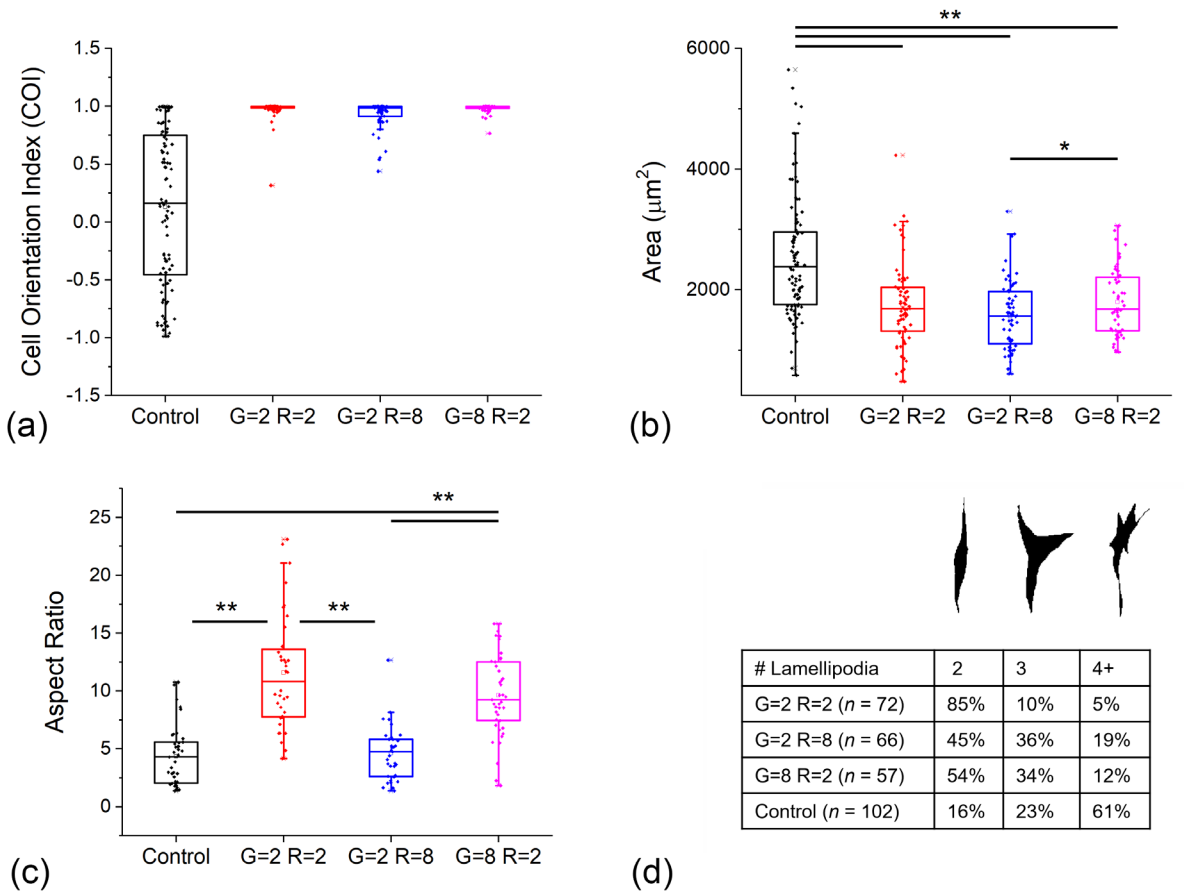

# Lamellipodia	2	3	4+
G=2 R=2 (*n* = 72)	85%	10%	5%
G=2 R=8 (*n* = 66)	45%	36%	19%
G=8 R=2 (*n* = 57)	54%	34%	12%
Control (*n* = 102)	16%	23%	61%

Fig. 3 — Cell Morphological Characterization. A) Cell Orientation Index (COI) B) Cell spread area C) Cell aspect ratio D) Number of lamellipodia classification for each topographical condition. All measurements were taken 6 hours after initial cell plating, * denotes $p < 0.05$ and ** $p < 0.005$ via Mann-Whitney test.

Cell Migration

All of the SiO_2 topographies greatly altered the migratory patterns of fibroblasts compared to flat SiO_2 controls, with Figure 3A-D showing the migration tracks of twenty cells per topographical condition. Cells on the flat SiO_2 surface exhibited highly persistent, yet randomly oriented migration paths (Figure 3A). Cells on all topographical conditions exhibited a similarly persistent migration path, however migration was almost exclusively directed along the orientation of the topographical cues. The migration velocity of all topographical conditions was approximately 25 μm/hr and did not alter significantly (Figure 3E), similarly with migration distance traveled (~ 350μm). The directionality, however, was significantly higher on topographies with smaller ridges (R=2, Figure 3F) compared to flat controls or R=8 topographies.

To better understand how the fibroblasts interact with the topographical cues, high magnification Interference Reflection Microscopy (IRM) was employed to assess lamellipodia dynamics. IRM is a technique that visualizes interference patterns generated from reflections of an incident light beam as it passes through materials of different refractive indices. In the context of cells on a glass surface in a liquid medium, the intensity of these interference patterns is indicative of the distance between the cell and the glass surface19. Due to this enhanced visibility into the cell-surface interface, IRM has been a useful optical modality to study cell adhesion and motility 20. Figure 4A-C shows typical high resolution

IRM images of fibroblast on topographies. Generally, cells on the smallest topographical condition (G=2 R=2) were observed to have lamellipodia equally on both the etched grooves and unetched ridges (white arrows, Figure 4A), despite possessing extremely elongated morphologies and relatively high speeds of lamellipodia extension/retraction. Cells on the G = 2 R = 8 topographies typically had lamellipodia preferentially extended along the wider unetched ridges, with the lamellipodia often assuming a semi-circular geometry on the top ridges confined by the surrounded grooves (white arrows, Figure 4B). Similarly, cells on the G=8 R=2 topographies had lamellipodia predominantly on the wider etched grooves in which the lamellipodia were typically confined into single grooves by the surrounding ridges (white arrows, Figure 4C).

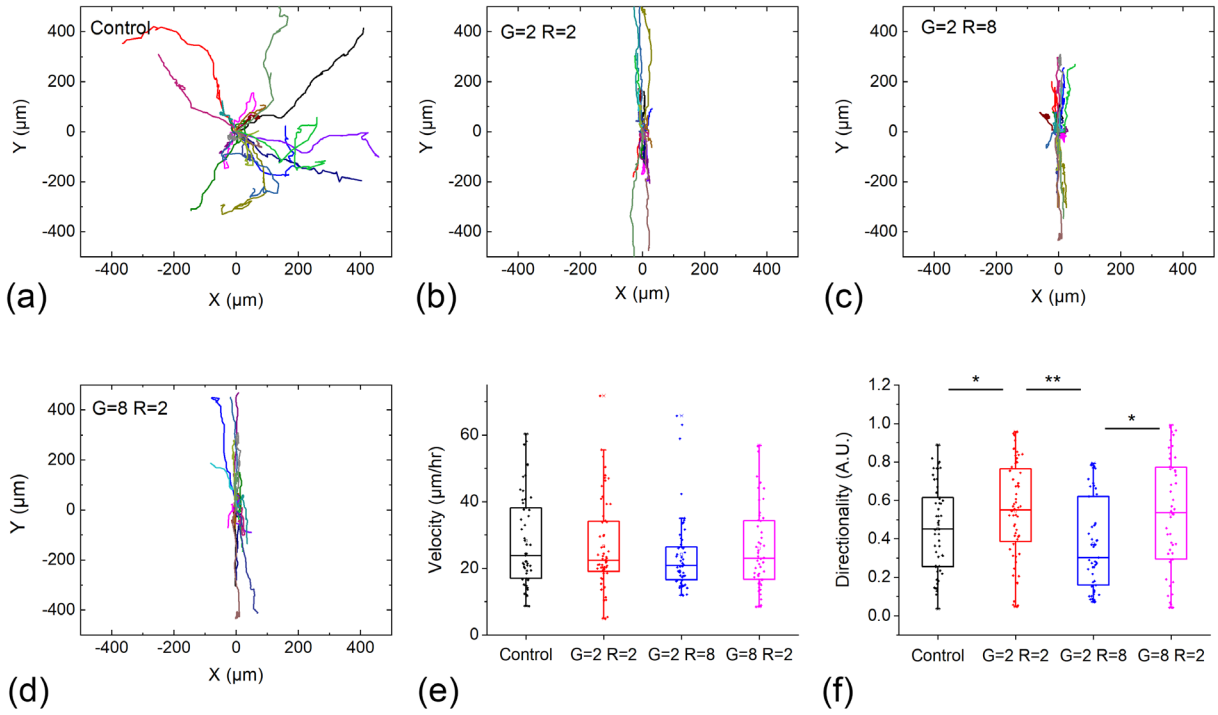

Fig. 4 — Cell Migration Characterization. A)-D) 20 migration tracks of fibroblasts on each topographical condition. E) Cell speed and F) Cell migration directionality box plots for each topographical condition.

Immunostaining

At the end of an experiment (18 hours), the fibroblasts were fixed and immunostained for both vinculin and actin to characterize focal adhesion and stress fiber distribution, respectively. In general, we observed fewer fibroblasts on SiO2 topographies that had mature focal adhesions via vinculin staining compared to fibroblasts on flat control areas. Focal adhesion area on both flat control areas and topographies exhibited a fairly large variance, and was slightly larger on flat controls or topographies with wider grooves G = 8 (Figure 4H). Focal adhesion morphology was consistent across all topographical conditions, exhibiting an elongated morphology with an eccentricity ~0.7-0.9, with focal adhesions on flat controls or R = 2 G = 2 topographies having a slightly higher eccentricity compared to topographies with ridges or grooves of 8 µm (Figure 4I). Focal adhesion orientation angle, with 90° being aligned with the topographical cues and 0° being perpendicular, was approximately 45° with an even distribution indicating random alignment for cells on flat control areas (Figure 5J). Cells on etched topographies had a tighter distribution of focal adhesion orientation of approximately 80°, indicating high alignment with

topographies. Mature stress fibers were observed in all fibroblasts that exhibited mature focal adhesions, with the ends of stress fibers anchored by focal adhesions (Figure 5D-G). The orientation of stress fibers followed that of focal adhesions; randomly oriented on flat control areas and tightly aligned with focal adhesions/groove orientation on the etched topographies.

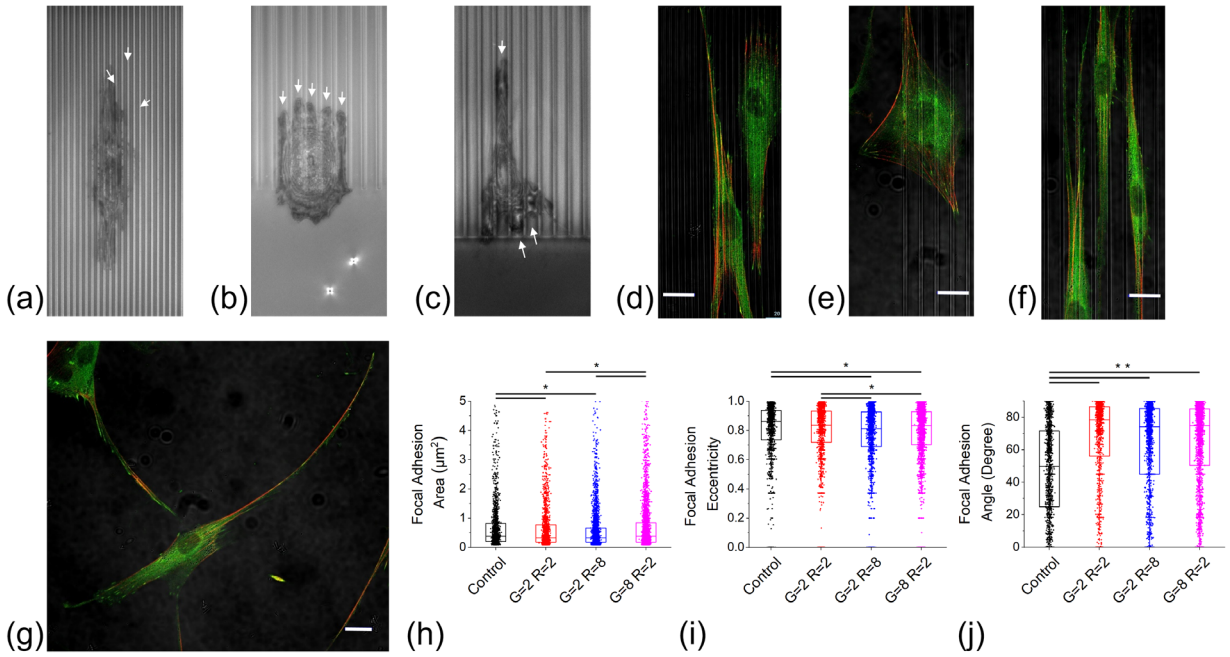

Fig. 5 — Cell Focal Contacts/Adhesion Characterization. Representative IRM images of fibroblasts on A) G = 2 R = 2 topography highlighting even distribution of filopodia on both ridges and grooves (white arrows) B) G = 2 R = 8 topography highlighting lamellipodia preferentially located on wider ridges (white arrows). C) G = 8 R = 2 topography highlighting lamellipodia preferentially located on wider etched grooves (white arrows). Representative confocal images highlighting focal adhesion (vinculin, green) and stress fiber (actin, red) on D) G = 2 R = 2 topography E) G = 2 R = 8 topography F) G = 8 R = 2 topography and G) flat SiO_2 control. Box plots of measured focal adhesion H) Area I) Eccentricity and J) Orientation angle, * denotes $p < 0.05$ and ** $p < 0.005$ via Mann-Whitney test. Scale bar = 20 μm.

CONCLUSIONS

Cell adhesion and migration is a crucial aspect to wound healing, and by understanding how the physical properties of in vitro environments effect these basic cellular processes, the closer we are to implementing wound healing materials with optimized physical properties in vivo. In two dimensions, adhesion and migration typically involves actin polymerization that drives lamellipodia or protrusions outward from the cell membrane, and new focal adhesions form underneath the expanding edges allowing for motion. Here, the cells exhibited smaller spread area on all topographies compared to flat control areas, with only topographies of wider grooves having slightly larger spread area compared to other topographical conditions (Figure 3B). All of the topographical conditions resulted in high cell orientation parallel to the cues, as well as focal adhesion and stress fiber alignment which is consistent with previous findings [21, 22]. Furthermore, these results support the explanation that the anisotropy of the underlying substrate physically constrains focal adhesion maturation, thereby constraining actin organization and subsequent force generation along the direction of the substrate anisotropy [23]. Indeed, all topographical conditions explored in this study resulted in highly oriented migration directions along the direction of the topographical anisotropy (Figure 4B-D). This fits well into the general perspective that if the formation of new focal adhesions themselves are directionally persistent, the cell will move in a directionally persistent manner [8, 24]. The highly multiplexed nature of our contact guidance chips, with 16 different topographies per chip, enabled this data to be efficiently gathered on dozens of cells over the course of one or two passages.

Cells on topographies with ridge length of R = 2 μm exhibited a significantly elongated morphology compared to flat controls or R = 8 μm topographies (Figure 3C). This may suggest the relatively larger role that ridge geometrical confinement plays with regards to cell protrusions/morphology compared to groove confinement at a given groove depth. Indeed, relaxing the ridge topographical constraint by a factor of four (i.e. R = 2 → R =8) also correlated with a reduction in migration directionality (Figure 4F), however this did not correlate with any significant changes in fibroblast speed or orientation.

Focal adhesion area was observed to be slightly higher for flat controls or topographies with larger grooves (G = 8, Figure 4H). Given that the smallest topographical feature (grooves or ridges of 2 μm) is larger than the average focal adhesion area of ~ 0.4 μm^2, it is likely that the topographical cues can only influence the orientation of focal adhesions but do not span to small enough dimensions to greatly alter the focal adhesion size itself. This lack of focal adhesion area-variation may also shed light as to consistent migration velocities observed on all topographical and control conditions. Kim and Wirtz have hypothesized that focal adhesion size can greatly influence migration speed [25]. The results here are consistent with this view, albeit almost in the form of a control, in which no large changes in focal adhesion size across multiple topographical cues results in no significant changes in migration speed. We note that the optical-based lithographic approach used to pattern the chips in this study is readily replaced by electron-beam lithography which has the resolution to reduce G and R values to tens of nanometers. This nanoscale version of the current chip will be the focus of future work.

Cellular response to topographical cues is heavily cell type and phenotype dependent [8, 9, 23]. Thus, there is a need for a uniform topographical platform in order to make sure that the in-vitro *context* of the topographical cues in question are presented the same, so researchers are confident that the measured responses are due to fundamental mechanisms instead of due to experimental variations. Indeed, the variables in question form quite a large parameter phase-space, including topographical geometry, surface roughness, amount of adsorbed protein, and cell media contents/reagents to name a few. This initial study spanned a range of topographical features large enough to elicit different Hs27 morphological responses but too small to observe any changes in migratory response from the cells. Future work will focus expanding the topographical cues to account for different etch depths as well as variation in adsorbed proteins to establish a complete phase diagram of the response of Hs27 fibroblasts (or any cell type in general) to topographical cues.

In this program we have introduced a novel method for precise fabrication of monolithic topographical features for in vitro studies via etched SiO_2. This fabrication technique allows for tight control in the topographical features across the sample and deep etching into SiO_2 (depth > 1 μm). By using commercially available quartz coverslips, these chips can easily integrate into virtually any optical modality for in-vitro experiments, and offers a platform with well characterized surfaces in terms of roughness and adsorption of relevant proteins typically required in live cell experiments. The quartz chip surface can easily be regenerated, and possesses a large enough surface area to accommodate a multiplexed topographical assay. The topographical platform was validated with Hs27 fibroblasts utilizing both standard (phase contrast, confocal) and more specialized (IRM) microscopy techniques. This method offers versatile range in etched topographies, integration with diverse optical modalities, means to characterize surface environments making it an ideal candidate to serve as a standard in vitro topography platform and to generally investigate fundamental mechanisms governing cellular response to topographical cues.

REFERENCES

1. J. Li, J. Chen and R. Kirsner: Pathophysiology of acute wound healing. *Clinics in dermatology* **25**, 9 (2007).
2. D. Newgreen: Physical influences on neural crest cell migration in avian embryos: contact guidance and spatial restriction. *Developmental biology* **131**, 136 (1989).
3. P.P. Provenzano, K.W. Eliceiri, J.M. Campbell, D.R. Inman, J.G. White and P.J. Keely: Collagen reorganization at the tumor-stromal interface facilitates local invasion. *BMC medicine* **4**, 38 (2006).
4. P. Clark, P. Connolly, A. Curtis, J. Dow and C. Wilkinson: Topographical control of cell behaviour: II. Multiple grooved substrata. *Development* **108**, 635 (1990).
5. A.I. Teixeira, G.A. McKie, J.D. Foley, P.J. Bertics, P.F. Nealey and C.J. Murphy: The effect of environmental factors on the response of human corneal epithelial cells to nanoscale substrate topography. *Biomaterials* **27**, 3945 (2006).
6. M.S. Lord, M. Foss and F. Besenbacher: Influence of nanoscale surface topography on protein adsorption and cellular response. *Nano Today* **5**, 66 (2010).
7. A.M. Ross, Z. Jiang, M. Bastmeyer and J. Lahann: Physical aspects of cell culture substrates: topography, roughness, and elasticity. *Small* **8**, 336 (2012).
8. M.J.P. Biggs, R.G. Richards and M.J. Dalby: Nanotopographical modification: a regulator of cellular function through focal adhesions. *Nanomedicine: Nanotechnology, Biology and Medicine* **6**, 619 (2010).
9. E. Martinez, E. Engel, J. Planell and J. Samitier: Effects of artificial micro-and nano-structured surfaces on cell behaviour. *Annals of Anatomy-Anatomischer Anzeiger* **191**, 126 (2009).
10. A.-S. Andersson, F. Bäckhed, A. von Euler, A. Richter-Dahlfors, D. Sutherland and B. Kasemo: Nanoscale features influence epithelial cell morphology and cytokine production. *Biomaterials* **24**, 3427 (2003).
11. J.L. Charest, L.E. Bryant, A.J. Garcia and W.P. King: Hot embossing for micropatterned cell substrates. *Biomaterials* **25**, 4767 (2004).
12. W. Loesberg, J. Te Riet, F. Van Delft, P. Schön, C. Figdor, S. Speller, J. Van Loon, X. Walboomers and J. Jansen: The threshold at which substrate nanogroove dimensions may influence fibroblast alignment and adhesion. *Biomaterials* **28**, 3944 (2007).

13. S. Heydarkhan-Hagvall, C.-H. Choi, J. Dunn, S. Heydarkhan, K. Schenke-Layland, W.R. MacLellan and R.E. Beygui: Influence of systematically varied nano-scale topography on cell morphology and adhesion. *Cell communication & adhesion* **14**, 181 (2007).
14. C. Miller, H. Shanks, A. Witt, G. Rutkowski and S. Mallapragada: Oriented Schwann cell growth on micropatterned biodegradable polymer substrates. *Biomaterials* **22**, 1263 (2001).
15. J.B. Recknor, J.C. Recknor, D.S. Sakaguchi and S.K. Mallapragada: Oriented astroglial cell growth on micropatterned polystyrene substrates. *Biomaterials* **25**, 2753 (2004).
16. M.V. Voinova, M. Rodahl, M. Jonson and B. Kasemo: Viscoelastic acoustic response of layered polymer films at fluid-solid interfaces: continuum mechanics approach. *Physica Scripta* **59**, 391 (1999).
17. A.E. Carpenter, T.R. Jones, M.R. Lamprecht, C. Clarke, I.H. Kang, O. Friman, D.A. Guertin, J.H. Chang, R.A. Lindquist and J. Moffat: CellProfiler: image analysis software for identifying and quantifying cell phenotypes. *Genome biology* **7**, R100 (2006).
18. P.A. Dimilla, S.M. Albelda and J.A. Quinn: Adsorption and elution of extracellular matrix proteins on non-tissue culture polystyrene petri dishes. *Journal of colloid and interface science* **153**, 212 (1992).
19. A. Curtis: The mechanism of adhesion of cells to glass: a study by interference reflection microscopy. *The Journal of cell biology* **20**, 199 (1964).
20. K. Klein, C.E. Rommel, V.C. Hirschfeld-Warneken and J.P. Spatz: Cell membrane topology analysis by RICM enables marker-free adhesion strength quantification. *Biointerphases* **8**, 28 (2013).
21. A.I. Teixeira, G.A. Abrams, P.J. Bertics, C.J. Murphy and P.F. Nealey: Epithelial contact guidance on well-defined micro-and nanostructured substrates. *Journal of cell science* **116**, 1881 (2003).
22. M. Azatov, X. Sun, A. Suberi, J.T. Fourkas and A. Upadhyaya: Topography on a subcellular scale modulates cellular adhesions and actin stress fiber dynamics in tumor associated fibroblasts. *Physical biology* **14**, 065003 (2017).
23. A. Ray, O. Lee, Z. Win, R.M. Edwards, P.W. Alford, D.-H. Kim and P.P. Provenzano: Anisotropic forces from spatially constrained focal adhesions mediate contact guidance directed cell migration. *Nature communications* **8**, 14923 (2017).
24. R.J. Petrie, A.D. Doyle and K.M. Yamada: Random versus directionally persistent cell migration. *Nature reviews Molecular cell biology* **10**, 538 (2009).
25. D.-H. Kim and D. Wirtz: Focal adhesion size uniquely predicts cell migration. *The FASEB Journal* **27**, 1351 (2013).